line width, and that contributions from elastic processes also need to be considered.

In summary, neither Raman line widths and band shapes by themselves, nor direct measurement of state-to-state rates (because of the limited experimental accuracy of the latter), appear to be sufficient for a clear discrimination between the various fitting and scaling laws. The combination of several types of measurements, particularly including Raman Q-branch narrowing at high densities, and accurate and reliable measurement of collisional shifts, is necessary for a definitive test of the rate laws. The optimum procedure for determining rate laws and parameters would be a simultaneous, properly weighted, global fit of Raman linewidths, state-to-state rates (when available), and collision-narrowed SRS Q-branch bandshapes over a range of densities, taking proper account of collisional shifts as well. The development of such a procedure is currently in progress.[57] Furthermore, preliminary results at the Laboratoire de Spectronomie Moléculaire et Instrumentation Laser in Dijon[58] seem to indicate that high-resolution Coherent Anti-Stokes Raman Spectroscopy (CARS) is a little more sensitive than SRS to the type of model used to calculate the collision-narrowed Q-branch. It is likely that inclusion of high-resolution collision-narrowed CARS Q-branch data could further improve the suggested procedure.

Acknowledgment. Support for this work was provided in part by the Office of Standard Reference Data and Quantum Physics Division of the National Bureau of Standards (now NIST), and by the Advanced Laser Technology Division of the U.S. Air Force Weapons Laboratory. J.I.S. thanks Jean Gallagher, Steve Leone, and the staff of JILA and the Atomic Collisions Data Center for their assistance, hospitality, and enthusiasm during the initial stages of this work; the members of the Laboratoire de Spectronomie Moléculaire et Instrumentation Laser (SMIL) for their hospitality during a recent sabbatical visit; and the NASA Office of Space Science and Applications, Upper Atmosphere Research Program and Planetary Atmospheres Program, for their continuing support of our recent research. The Centre National de la Recherche Scientifique, Paris, and the Conseil Régional de Bourgogne are gratefully acknowledged for their financial support of the work at SMIL.

Registry No. N_2, 7727-37-9.

(57) Roche, C., unpublished results.
(58) Fanjoux, G., unpublished results.

ARTICLES

Role of Charge Transfer for the Vibrational-Mode-Specific Chemical Reaction of $NH_3^+(v)$ and NH_3

Akitomo Tachibana,*,† Susumu Kawauchi,†,‡,§ Yuzuru Kurosaki,† Naoto Yoshida,† Takeo Ogihara, and Tokio Yamabe†,‡

Department of Hydrocarbon Chemistry, Faculty of Engineering, Kyoto University, Kyoto 606, Japan
(Received: December 5, 1990; In Final Form: July 18, 1991)

New reaction pathways involving $(NH_3{\cdot}NH_3)^+$ charge-transfer (CT) complex formation have been proposed for the vibrational-mode-specific reaction of $NH_3^+(v)$ with NH_3 using the concept of a meta-IRC (intrinsic reaction coordinate). It is known experimentally for the reaction that there are three elementary processes, electron transfer (ET), proton transfer (PT), and hydrogen abstraction (HA). The CT complex formation plays a key role in our proposed reaction pathways for both ET and HA processes: in ET the reactants form the CT complex, which then dissociates to NH_3^+ and NH_3 with an electron transferred from one to the other, while in HA the CT complex does not dissociate but undergoes a rearrangement to form the $(NH_4{\cdot}NH_2)^+$, complex, which dissociates to NH_4^+ and NH_2. The overall HA process has been predicted to have no energy barrier and to be exothermic by 15.8 kcal/mol at the HF/4-31G level of calculation. We have suggested that three characteristic transition points (TP's) exist for the reaction pathway of HA: (1) the "primary" TP of the CT process prerequisite for the HA to occur, (2) the geographical TP of the potential surface, i.e., the conventional transition state (TS) for the HA process, and (3) the "secondary" TP of the geometrical change for the HA process. For the ordinary reaction coordinate, the conventional TS merges the TP of CT and the geometrical TP, but in this case the character of the conventional TS splits into the three TP's. In particular, we have found that the CT process around the primary TP is most significant for the vibrational-mode specificity of the ET and HA processes. Moreover, our mechanism elucidates the non-state-selected experimental results: the reaction proceeds via PT (85%) rather than HA (15%) and ET is negligible.

Introduction

Three elementary processes, proton transfer (PT), hydrogen abstraction (HA), and electron transfer (ET),[1] in the reaction of neutral ammonia NH_3 and vibrationally excited ammonia cation $NH_3^+(v)$ have been studied state selectively.[2] It has been found that PT is suppressed while HA and ET are enhanced by the excitation of v_2 umbrella-bending vibrational mode of the NH_3^+.[2e,f]

TABLE I: Total Energies[a] (au)

species	energy	species	energy
NH_3	-56.106692	$(NH_3{\cdot}NH_3)^+$	-111.952851
NH_3^+	-55.801670	$(NH_4{\cdot}NH_2)^+$	-111.977768
NH_4^+	-56.458884	TS	-111.944909
NH_2	-55.474727		

[a] At the HF/4-31G level.

† Additional address: Division of Molecular Engineering, Graduate School of Engineering, Kyoto University, Kyoto 606, Japan.
‡ Additional address: Institute for Fundamental Chemistry, 34-4 Nishihiraki-cho, Takano, Sakyo-ku, Kyoto 606, Japan.
§ On leave from Kawasaki Plastics Laboratory, Showa Denko K. K., Kawasaki 210, Japan.

0022-3654/91/2095-9647$02.50/0

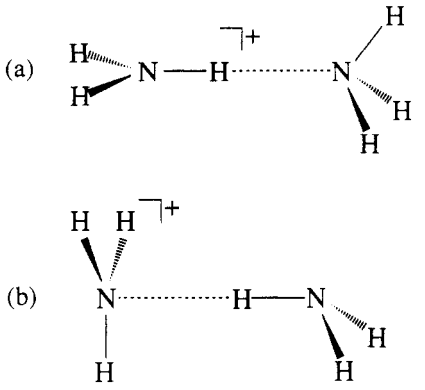

Figure 1. Hydrogen-bond models for (a) the PT process and (b) the HA process proposed by Conaway et al.[1e] and Tomoda et al.[1f]

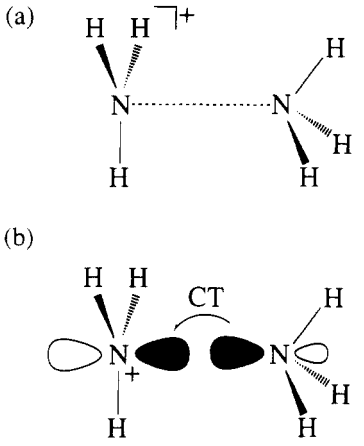

Figure 2. (a) Present model for HA process and (b) its HOMO–LUMO interaction.

In order to elucidate the vibrational-mode specificity, Conaway et al.[2e] and Tomoda et al.[2f] proposed the hydrogen-bond-type conformations of NH_3^+ and NH_3 as reaction models for the PT and HA process (Figure 1). Conaway et al.[2e] interpreted this vibrational-mode specificity in terms of the coincidence between the direction of the v_2 vibrational motion of NH_3^+ and that of the reaction pathway as shown in Figure 1; the vibrational motion is orthogonal to the reaction pathway of PT but is parallel to that of HA. The hydrogen-bond model (Figure 1a) can explain consistently the PT process suppressed by the excitation of the v_2 vibrational mode of NH_3^+. Tomoda et al.[2f] claimed that the ground-state potential surface is quite favorable for PT to occur without an activation barrier and HA should have a barrier corresponding to an electron jump followed by PT. Indeed, several workers[3] have observed by the non-state-selected studies that the reaction proceeds via PT rather than HA; e.g., Adams et al.[3c] showed by using the selected ion flow tube (SIFT) technique that in the $ND_3^+ + NH_3$ system PT is a dominant reaction pathway (85%) and the remaining 15% corresponds to HA. In addition, it is noteworthy that, under thermal conditions, ET is negligible ($k = 4 \times 10^{-11}$ cm^3 mol^{-1} s^{-1}).[3a] We would like to claim that, in terms of orbital interaction, the overlap of the HOMO of NH_3 and the LUMO of NH_3^+ of the hydrogen-bond model for HA (Figure 1b) is not large enough for the electron jump to occur.

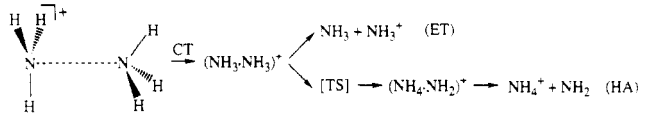

Figure 3. Reaction scheme for the present mechanisms of the ET and HA processes.

Therefore, it may not be expected that the vibrational-mode specificity observed in HA is explained well by their mechanisms.

In the present paper, we adopted an initial conformation of the reactants for HA as shown in Figure 2, instead of the hydrogen-bond model (Figure 1b), because our model seems more favorable for the in-phase overlap of the HOMO of NH_3 and the LUMO of NH_3^+ in terms of orbital interaction. The orbital interaction between the HOMO of NH_3 and the LUMO of NH_3^+ is also illustrated in the figure. Our model must lead to the $(NH_3{\cdot}NH_3)^+$ charge-transfer (CT) complex formation. Actually, it has recently been observed both experimentally[4] and theoretically[5] that the CT complex $(NH_3{\cdot}NH_3)^+$ is a metastable intermediate. Furthermore, Gill and Radom[5b] have studied the rearrangement and dissociative process for the $(NH_3{\cdot}NH_3)^+$ theoretically in terms of two-center three-electron (2c-3e) bonds. They have considered not $(NH_3{\cdot}NH_3)^+$ but $(NH_4{\cdot}NH_2)^+$ as a key complex for both PT and ET processes and they have not referred to HA. However, the CT complex $(NH_3{\cdot}NH_3)^+$ seems to act as a reaction intermediate not only for HA but also for ET as shown in Figure 3: in ET the reactants form the CT complex, which then dissociates to NH_3^+ and NH_3 with an electron transferred from one to the other, while in HA the CT complex does not dissociate but undergoes a rearrangement to form the $(NH_4{\cdot}NH_2)^+$ complex, which dissociates to NH_4^+ and NH_2. Therefore, in this paper we try to clarify the role of the CT complex formation for the vibrational mode specific reaction of $NH_3^+(v)$ with NH_3 using the concept of a meta-IRC (intrinsic reaction coordinate).[6]

The IRC defines for chemically reacting systems an idealized locus of nuclei on the adiabatic potential energy surface; the IRC is a curve passing from the initial to the final basin (or valley) by way of the transition state (TS) on the surface.[6,7] The meta-IRC is an extended version of the IRC even for the reaction having no TS and no activation barrier and is among an infinite number of solutions of the IRC equation.[6] The meta-IRC can be selected voluntarily and corresponds to the reaction coordinate starting from a given vibrationally excited state. We apply the meta-IRC for the CT complex $(NH_3{\cdot}NH_3)^+$ formation from the two separate reactants, NH_3^+ and NH_3. Then we adopt the IRC for HA, which starts from the $(NH_3{\cdot}NH_3)^+$ complex to the $(NH_4{\cdot}NH_2)^+$ complex proceeding via a TS on the potential energy surface, and the frequency of the normal vibrational modes orthogonal to the IRC[8] is calculated in order to discuss the influence of molecular vibration on the reaction dynamics.

Methods of Calculation

We performed molecular orbital (MO) calculations with the GAUSSIAN82 program[9] at the restricted and unrestricted Hartree–Fock (RHF and UHF) levels by using the standard split-valence 4-31G[10] basis set. The geometries were fully optimized

(1) Although the term "charge transfer" has been used traditionally (for example, refs 2 and 3) for the reaction: $NH_3^+ + NH_3 \rightarrow NH_3 + NH_3^+$, the term "electron transfer" was used throughout the paper in order to distinguish from the charge transfer reaction $NH_3^+ + NH_3 \rightarrow (NH_3{\cdot}NH_3)^+$.

(2) (a) Chupka, W. A.; Russell, M. E. *J. Chem. Phys.* **1968**, *48*, 1527. (b) Sieck, L. W.; Hellner, L.; Gordon, R., Jr. *Chem. Phys. Lett.* **1971**, *10*, 502. (c) Baer, T.; Murray, P. T. *J. Chem. Phys.* **1981**, *75*, 4477. (d) Van Pijkeren, D.; Van Eck, J.; Niehaus, A. *Chem. Phys.* **1985**, *95*, 449. (e) Conaway, W. E.; Ebata, T.; Zare, R. N. *J. Chem. Phys.* **1987**, *87*, 3453. (f) Tomoda, S.; Suzuki, S.; Koyano, I. *Ibid.* **1988**, *89*, 7268.

(3) (a) Huntress, W. T.; Mosesman, M. M.; Elleman, D. D. *J. Chem. Phys.* **1970**, *54*, 843. (b) Huntress, W. T.; Pinizzotto, R. F., Jr. *Ibid.* **1973**, *59*, 4742. (c) Adams, N. G.; Smith, D.; Paulson, J. F. *Ibid.* **1980**, *72*, 288.

(4) Ganghi, N.; Wyatt, J. L.; Symons, M. C. R. *J. Chem. Soc., Chem. Commun.* **1986**, 1424.

(5) (a) Bouma, W. J.; Radom, L. *J. Am. Chem. Soc.* **1985**, *107*, 345. (b) Gill, P. M. W.; Radom, L. *Ibid.* **1988**, *110*, 4931.

(6) Tachibana, A.; Fukui, K. *Theor. Chim. Acta* **1978**, *49*, 321; **1979**, *51*, 189; **1979**, *51*, 275; **1980**, *57*, 81.

(7) (a) Fukui, K. *J. Phys. chem.* **1970**, *74*, 4161. (b) Fukui, K. *Acc. Chem. Res.* **1981**, *14*, 363. (c) Garrett, B. C.; Redmon, M. J.; Steckler, R.; Truhlar, D. G.; Baldridge, K. K.; Bartol, D.; Schmidt, M. W.; Gordon, M. S. *J. Phys. Chem.* **1988**, *92*, 1476. (d) Baldrige, K. K.; Gordon, M. S.; Steckler, R.; Truhlar, D. G. *Ibid.* **1989**, *93*, 5107.

(8) Miller, W. H.; Handy, N. C.; Adams, J. E. *J. Chem. Phys.* **1980**, *72*, 99.

(9) Binkley, J. S.; Frisch, M. J.; DeFrees, D. J.; Raghavachari, K.; Whiteside, R. A.; Schlegel, H. B.; Fluder, E. M.; Pople, J. A. GAUSSIAN 82, Release A version (Sept 1983); An Ab Initio Molecular Orbital Program, Carnegie-Mellon University, Pittsburgh, PA.

TABLE II: Relative Energies for the HA Process (kcal/mol)

	$NH_3 + NH_3^+$	→	$(NH_3{\cdot}NH_3)^+$	→	TS	→	$(NH_4{\cdot}NH_2)^+$	→	$NH_4^+ + NH_2$
HF/4-31G[a]	0		-27.9		-22.9		-43.6		-15.8
HF/6-31G*[b,c]	0		-24.2		-21.4		-41.7		-19.4
HF/6-31G**[d]	0		-23.7				-41.2		-18.8
MP2/6-31G*[b,e]	0		-40.3		-26.3		-46.1		-20.7
MP3/6-31G*[d]	0		-37.2				-45.6		-21.2
MP4/6-31G*[b,e]	0		-39.1		-26.3		-45.7		-21.2
MP2/6-311G**[b,e]	0		-38.1		-25.2		-43.7		-18.7

[a] Present work at HF/4-31G optimized structures. [b] Reference 5b. The $(NH_4{\cdot}NH_2)^+$ complex is in a staggered form. [c] At HF/6-31G* optimized structures. [d] Reference 5a at HF/6-31G* optimized structures. The $(NH_4{\cdot}NH_2)^+$ complex is in an eclipsed form. [e] At MP2/6-31G* optimized structures.

in their own symmetry by the energy-gradient method.[11] The optimized geometries were characterized by the harmonic vibrational frequencies computed by using the analytical second derivatives[12] based on the HF method: i.e., a local minimum has all positive eigenvalues but a saddle point (TS) has one negative eigenvalue and all the rest are positive. The meta-IRC and IRC calculations were carried out at the HF/4-31G level in the mass-weighted Cartesian coordinate system using the GAMESS program.[13] The meta-IRC was traced with a step size of 0.01 $amu^{1/2}$ bohr. The step size employed for the IRC calculation was as follows (the unit is $amu^{1/2}$ bohr): 0.005 ($-3.0 \le s \le -0.05$); 0.05 ($-0.05 \le s \le 0.05$); 0.005 ($0.05 \le s \le 3.5$), where s is the mass-weighted Cartesian coordinate. Frequencies of the vibrational modes orthogonal to the IRC were obtained by diagonalizing the projected force constant matrix projecting out the degrees of freedom of the IRC, overall translations and rotations.[8]

Results and Discussion

Proposed Mechanism for the HA and ET Processes. The CT complex $(NH_3{\cdot}NH_3)^+$ seems to act as a reaction intermediate not only for HA but also for ET (Figure 3), because the orbital interaction between the HOMO of NH_3 and the LUMO of NH_3^+ for the proposed model (Figure 2) is advantageous over the hydrogen-bond model (Figure 1b) proposed by Conaway et al.[2e] and Tomoda et al.[2f] In this section, we will discuss the potential energy surface for the proposed model of the HA and ET processes.

The optimized geometries and the total energies of the fragments, the complexes, and the TS for the HA process at the HF/4-31G level are shown in Figure 4 and Table I, respectively. Relative energy values including the results at higher levels of calculation[5] are listed in Table II.

The geometry of the CT complex $(NH_3{\cdot}NH_3)^+$ optimized at the HF/4-31G level has D_{3d} symmetry (Figure 4e). The geometrical parameters agree well with the results at higher levels of calculation.[5] In the product region, NH_4^+ and NH_2 also form a stable $(NH_4{\cdot}NH_2)^+$ complex which has C_s symmetry. Considering the structure of the TS of the potential surface for HA, which will be discussed below, it is reasonable that this complex has a staggered form as shown in Figure 4f, where NHN is collinear and the nitrogen center of the right-hand side is planar. Vibrational analysis for the complex shows that it has an unstable normal mode with a small imaginary frequency (18.4i cm^{-1}) corresponding to the contrary rotations of the NH_3 and NH_2 groups around the HNH axis. This suggests that an instability[14] is brought about on the reaction pathway of HA in the vicinity of the complex in the product region, leading to the formation of a stable eclipsed-form complex as shown in Figure 4g, where

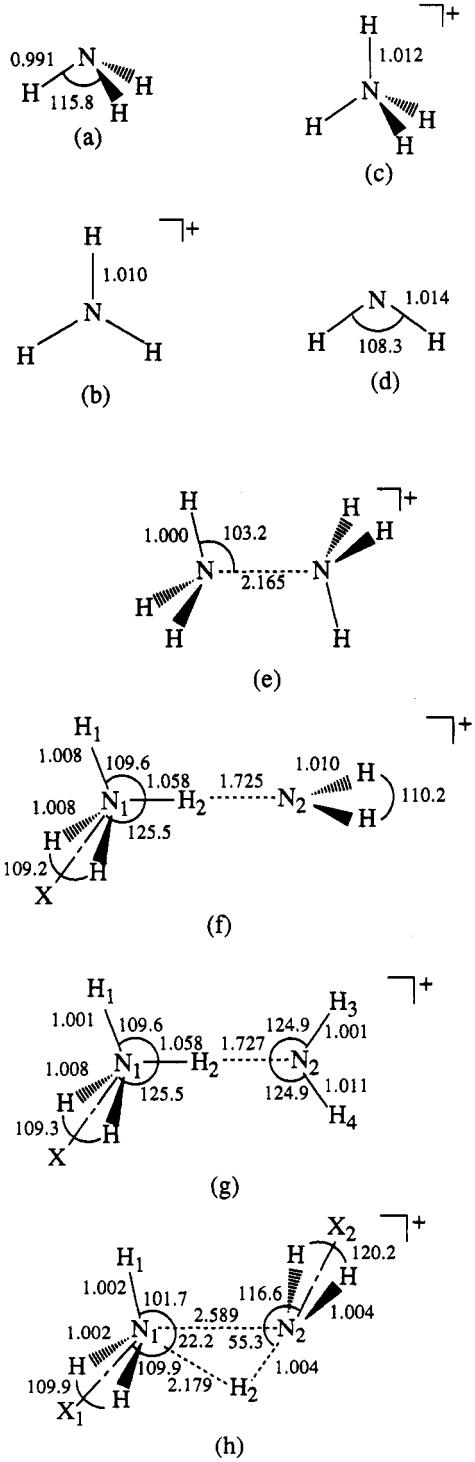

Figure 4. Optimized geometries of (a) NH_3 (C_{3v}), (b) NH_3^+ (C_{3h}), (c) NH_4^+ (T_d), (d) NH_2 (C_{2v}), (e) $(NH_3{\cdot}NH_3)^+$ complex (D_{3d}), (f) staggered $(NH_4{\cdot}NH_2)^+$ complex (C_s), (g) eclipsed $(NH_4{\cdot}NH_2)^+$ complex (C_s), and (h) TS (C_s). Bond lengths and angles are given in angstroms and degrees, respectively.

(10) Ditchfield, R.; Hehre, W. J.; Pople, J. A. *J. Chem. Phys.* **1971**, *54*, 724.
(11) Pulay, P. In *Modern Theoretical Chemistry*; Schaefer, H. F., III, Ed.; Plenum: New York, 1977; Vol. 4, Chapter 4.
(12) Pople, J. A.; Krishnan, R.; Schlegel, H. B.; Binkley, J. S. *Int. J. Quantum Chem. Symp.* **1979**, *13*, 225.
(13) Dupuis, M.; Spangler, D.; Wendoloski, J. J. GAMESS; NRCC Cat. Prog. QG01, 1980.
(14) (a) Tachibana, A.; Okazaki, I.; Koizumi, M.; Hori, K.; Yamabe, T. *J. Am. Chem. Soc.* **1985**, *107*, 1190. (b) Tachibana, A.; Fueno, H.; Yamabe, T. *J. Am. Chem. Soc.* **1986**, *108*, 4346.

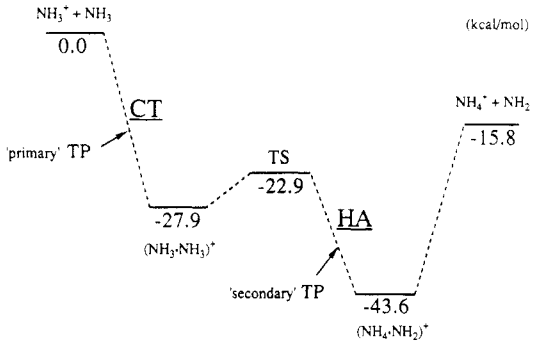

Figure 5. Energy diagram of the HA proces.

NHN is also collinear. The geometrical parameters for the $(NH_4 \cdot NH_2)^+$ complex agree quite well with those obtained at higher levels of calculation.[5] There is no energy difference between the staggered and eclipsed $(NH_4 \cdot NH_2)^+$ complexes. The geometrical parameters for the staggered complex reported by Tomoda[15] are slightly different from ours, despite the use of the same method of calculation, i.e., HF/4-31G. The geometry obtained by Tomoda may not be fully optimized.

The fully optimized geometry of the TS for HA is shown in Figure 4h. Vibrational analysis showed that the frequency of the imaginary mode is 486.5i cm^{-1}. The structure has C_s symmetry. Hence, we can consider that the reaction pathway maintains the C_s symmetry in the course of reaction, but, as stated above, instability[14] of the reaction pathway may occur in the product region. Geometrical parameters for the TS agree well with those obtained at higher levels of calculation.[5] Therefore, we may be allowed to present a reliable discussion for the TS structure based on the HF/4-31G method below. Since the NN distance in the TS is quite long, 2.589 Å, it is clear that there are two groups easily distinguished. One is L-NH_3, whose geometry resembles that of neutral NH_3. The bond angle between the two symmetric N1H bonds is 109.9° and the angle between the N1H1 bond on the symmetry plane and the symmetric N1H bond is 109.8°. The other group is R-NH_3, whose geometry is almost planar and resembles NH_3^+. The three NH bonds of R-NH_3 bend inward and the bent angle is 8.1°. This fragment is located across the NN axis, where the angle between NN and N2H2 on the symmetry plane is 55.3°.

The relative energies of $(NH_3 \cdot NH_3)^+$, TS, $(NH_4 \cdot NH_2)^+$, and $NH_4^+ + NH_2$ estimated by the Møller–Plesset (MP) perturbation method[5] are about 13, 4, 2, and 5 kcal/mol lower than those in the present work, respectively. Hence the barrier from the $(NH_3 \cdot NH_3)^+$ complex is estimated to be about 10 kcal/mol higher than that in the present work. However, since our results qualitatively agree with these data including electron correlation effects, we will discuss the energetics at the HF/4-31G level in this section.

The energy diagram for the reaction (Figure 5) shows the pathways of HA. It can be clearly seen that the overall reaction has no energy barrier and the two complexes are identified as the local minima on hollows of the potential energy surface. The binding energies of $(NH_3 \cdot NH_3)^+$ and $(NH_4 \cdot NH_2)^+$ from their relevant fragment molecules are 27.9 and 27.8 kcal/mol, respectively. The stabilities of these complexes are remarkably large. Ceyer et al.[16] measured by a molecular beam–photoionization method that the binding energy of the $(NH_3 \cdot NH_3)^+$ complex is 0.79 eV (18.2 kcal/mol), which is smaller than our computational result. Tomoda and Kimura[17] suggested that the value of Ceyer et al.[16] may not be reliable for HA. The energy barrier from the complex in the reactant region is 5.0 kcal/mol. This barrier is small compared with the stabilization energy of the complex; therefore, it is very easy to get over the barrier to reach the product complex with an exothermicity of 15.7 kcal/mol. The overall reaction, $NH_3^+ + NH_3 \rightarrow NH_4^+ + NH_2$, is exothermic by 15.8 kcal/mol.

(15) Tomoda, S. *Chem. Phys.* **1986**, *110*, 431.
(16) Ceyer, S. T.; Tiedemann, P. W.; Mahan, B. H.; Lee, Y. T. *J. Chem. Phys.* **1979**, *70*, 14.
(17) Tomoda, S.; Kimura, K. *Chem. Phys. Lett.* **1985**, *121*, 159.

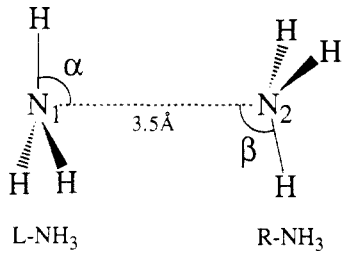

Figure 6. Geometry of the reaction system at the starting point (s = 0.0) of the meta-IRC for the HA process. L-NH_3 (R-NH_3) denotes the NH_3 fragment in the left-hand (right-hand) side which was originally NH_3^+ (NH_3).

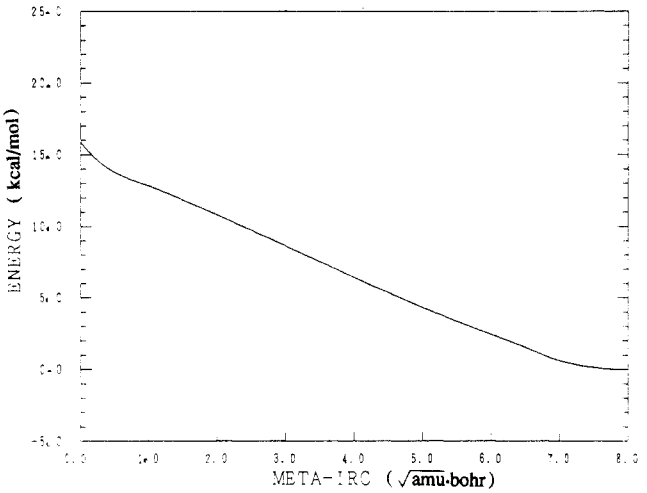

Figure 7. Potential energy profile along the meta-IRC for the CT process.

Meta-IRC for the CT Complex Formation. In order to explain the v_2 vibrational-mode specificity, we will propose here a new mechanism by using the meta-IRC concept. The meta-IRC for the CT complex $(NH_3 \cdot NH_3)^+$ has been traced from the geometry such that the isolated reactants, NH_3^+ and NH_3, are placed in a staggered C_{3v} conformation with the N–N distance being 3.5 Å (Figure 6) to the CT complex $(NH_3 \cdot NH_3)^+$. As described under Introduction, this model conformation of the reaction system favors a CT prerequisite for the HA process to occur, because the in-phase overlap of the HOMO of NH_3 and the LUMO of NH_3^+ is large (see Figure 2), while the hydrogen-bond-type model for HA proposed by both Conaway et al.[2e] and Tomoda et al.[2f] (Figure 1b) is clearly unfavorable for CT. Indeed, we tried to reproduce the hydrogen-bond-type conformation for the TS of the HA process but failed at the present level of calculation (HF/4-31G).

In Figure 7 is shown the potential energy profile for the CT complex formation along the meta-IRC. s = 0.0 corresponds to the starting geometry mentioned above. The rapid decrease of the potential energy around s = 0.0–0.5 may be due to the fact that the geometry at the starting point is somewhat artificial and is not significant for the present dynamics. The geometrical changes for the CT complex formation along the meta-IRC are shown in Figure 8. As shown in Figure 8a, the bond length N1N2 monotonously decreases along the meta-IRC, while the other bond lengths, N1H and N2H, remain almost constant. On the other hand, the bond angles, α and β, exhibit characteristic behavior (Figure 8b); α becomes smaller than 90° and β becomes larger than 101.9° in the range s = 1.0–5.0. Namely, the umbrella-bending motion of L-NH_3 (NH_3 fragment on the left-hand side which was originally NH_3^+) toward the N2 atom and that of R-NH_3 (NH_3 fragment on the right-hand side which was originally NH_3) have the same direction. The rapid changes of α and β around s = 0.0–0.5 are also due to the geometry at the starting point. Figure 9 schematically illustrates the geometrical change along the meta-IRC from the starting point to the

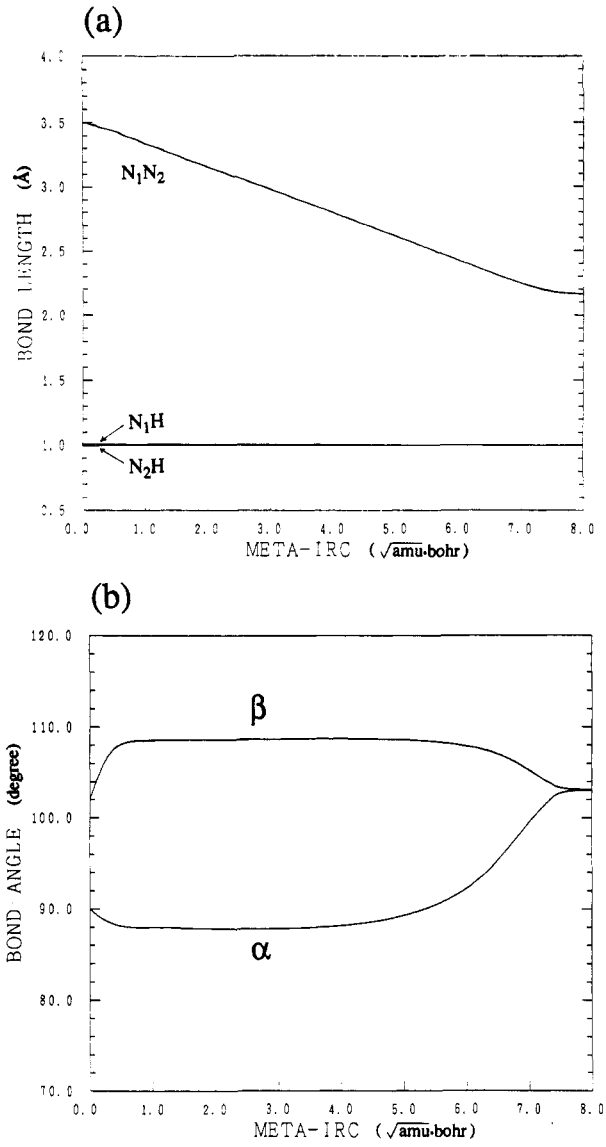

Figure 8. Geometrical changes along the meta-IRC for the CT process: (a) bond lengths and (b) bond angles.

$(NH_3{\cdot}NH_3)^+$ complex. The C_{3v} symmetry is retained along the meta-IRC. The CT complex formation reaction can be divided into two distinct steps by the transition point (TP) at $\alpha = 90°$ (see Figure 9). We call the TP the "primary" TP. In step 1, L-NH_3 and R-NH_3 bend in the same direction first, and then L-NH_3 begins to bend backward. It can be considered that the bending motions of hydrogens of L-NH_3 toward R-NH_3 is due to the electrostatic interaction between the positively charged hydrogens of L-NH_3 and the negatively charged nitrogen of R-NH_3. At the primary TP, which occurs around $s = 5.5$, α becomes about 90° and the N–N distance about 2.5 Å. In step 2, L-NH_3 bends in the direction opposite from N2, which finally leads to the $(NH_3{\cdot}NH_3)^+$ complex. In Figure 10 is shown the change of the Mulliken charge for L-NH_3 and R-NH_3 along the meta-IRC. Until the primary TP is reached CT occurs slowly, but after that it occurs very rapidly. Namely, the primary TP corresponds to the onset of the rapid CT. The meta-IRC is thus characterized by the electrostatic interaction followed by the CT.

As described under Introduction, the CT complex is an intermediate for ET or HA. Therefore, the vibrational-mode specificity in ET and HA can be explained as follows. The v_2 bending motion of NH_3^+ is parallel to the displacement vector of the meta-IRC. Also, the v_2 bending motion is considered to help the LUMO of NH_3^+ to overlap with the HOMO of NH_3, leading to CT from NH_3 to NH_3^+, which occurs rapidly from the primary TP. As a result, the excitation of the v_2 mode can promote both ET and HA. This is obviously consistent with the experimental results of the vibrational-mode specificity.[2]

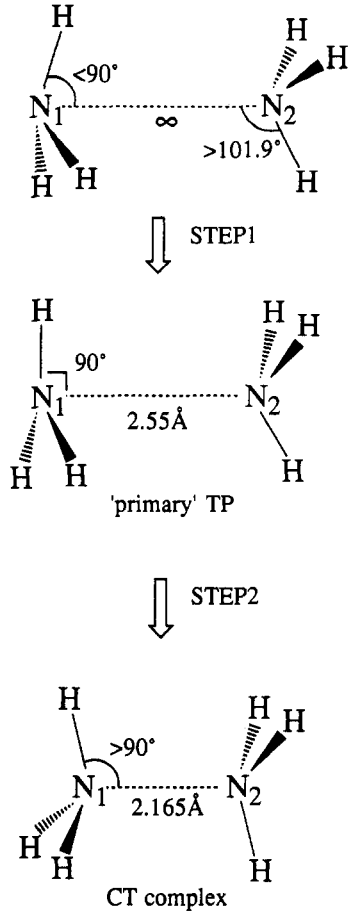

Figure 9. Schematic geometrical change along the meta-IRC for the CT process.

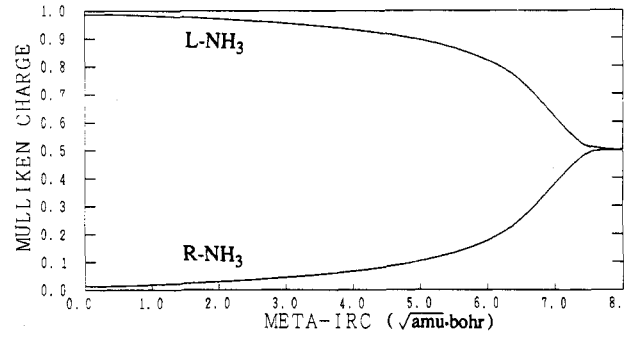

Figure 10. Change of Mulliken charge for L-NH_3 and R-NH_3 along the meta-IRC for the CT process.

IRC for the HA Process. In this section we will discuss the HA process along the IRC for HA from the $(NH_3{\cdot}NH_3)^+$ complex to the $(NH_4{\cdot}NH_2)^+$ complex via a TS of the potential energy surface. The potential energy profile along the IRC is shown in Figure 11. The origin of the IRC ($s = 0.0$) corresponds to the TS, the negative side the reactant region, and the positive side the product region. It is noteworthy that there is a shoulder around $s = 2.5$, where a transferring hydrogen is localized on the NN axis. Since the significant geometrical change occurs around this point, it can be referred to as the "secondary" TP for the present dynamics and will be discussed below.

In Figure 12 are shown the changes of geometrical parameters along the IRC for HA. It can be seen from Figure 12a that the bond length N1N2 increases gradually and N1H2 decreases rapidly in the course of the reaction, while N2H2 increases rapidly only in the product region. Considering a rapid decrease of the bond angle ∠N1N2H2 in the reactant region, which is shown in Figure 12b, as well as the bond-length behavior of N1H2, the early stage of this reaction can be mainly characterized by the transfer

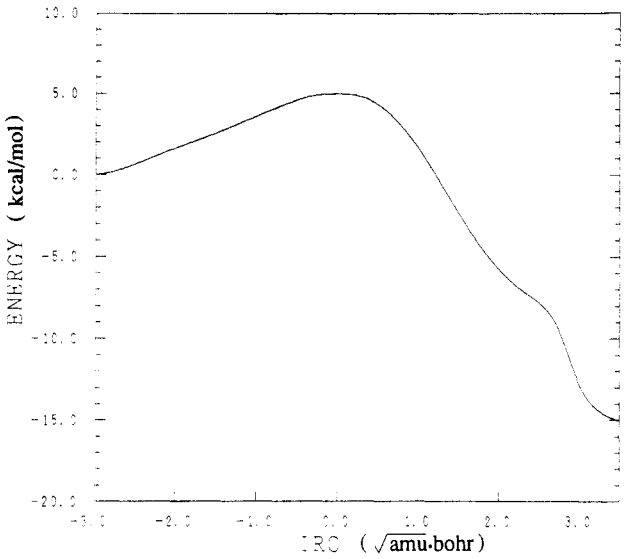

Figure 11. Potential energy profile along the IRC for the HA process.

of H2 toward the N1 atom. Around $s = -1.0$ the sum of the values of the angles ∠N1N2H2 and ∠X2N2N1 becomes about 180°, which indicates that R-NH_3 is almost planar. Of note is that the sum of the angles remains almost constant at 180° around the TS, indicating that the rotational motion of R-NH_3 is dominant in the reaction coordinate. Around $s = 2.5$, ∠N1N2H2 and ∠X2N2N1 become almost 0.0° amd 180°, respectively, and N2H2 begins to increase rapidly. For $s > 2.5$, N1N2 does not change much relative to the rapid change of N2H2. Namely, the last stage of the reaction can be characterized by H2 transfer from N2 to N1 on the NN axis. We can thus obtain a simple picture of the IRC for HA. The reaction is composed roughly of three steps: H2 transfer toward N1 in the early stage, rotational motion of R-NH_3 in the vicinity of the TS, and H2 transfer from N2 to N1 on the NN axis in the last stage.

Figure 13 shows the changes in the frequencies of the normal modes perpendicular to the IRC. The modes denoted *a* and *b* correspond to the stretching mode of R-NH_3 and the v_2 bending mode of L-NH_3, respectively. The vectors of these modes as well as the IRC at the TS are shown in Figure 14. The frequency of mode *a* shows the largest decrease in the product region. Hemce, this mode may be strongly coupled with the IRC after the TS. Consequently, excitation of the NH_3 stretching mode can enhance the reactivity of HA, although the effect of excitation of the NH_3 vibrational mode is not considered in the present study. The frequency of mode *b* does not show a remarkable change in the course of the reaction. Hence, it cannot be expected that the excitation of the v_2 mode of NH_3^+ affects the dynamics of HA along the IRC. We can thus conclude that the vibrational-mode specificity observed in HA is not attributed to the dynamics along the IRC but to the CT process along the meta-IRC discussed in the previous section. Around $s = 2.5$, the frequencies of several modes show remarkable changes. This is because the formation of the N1H2 bond and the dissociation of the N2H2 bond take place around $s = 2.5$ instead of around the TS. The shoulder of the potential profile shown in Figure 11 is also due to the geometrical change around $s = 2.5$. We can thus refer to this point as the secondary TP, which is the one for geometrical change. For the ordinary reaction coordinate, the TS merges the TP of CT and the geometrical TP as well as the geographical TP, but in this case the character of the TS splits into the three TP's.

Illustration of the Reaction between NH_3^+ and NH_3. In this section, we will show that our mechanism can explain the non-state-selected experimental results[3] for the reaction between NH_3^+ and NH_3 as well as the vibrational-mode-specific reaction[2] of $NH_3^+(v)$ and NH_3. Energy diagrams for HA, ET, and CT processes at the HF/4-31G level are shown in Figure 15.

As discussed above, the hydrogen-bond model is suitable for the PT process (Figure 1a). Figure 15a shows the PT process proceeds via $(NH_4{\cdot}NH_2)^+$ complex formation with no activation

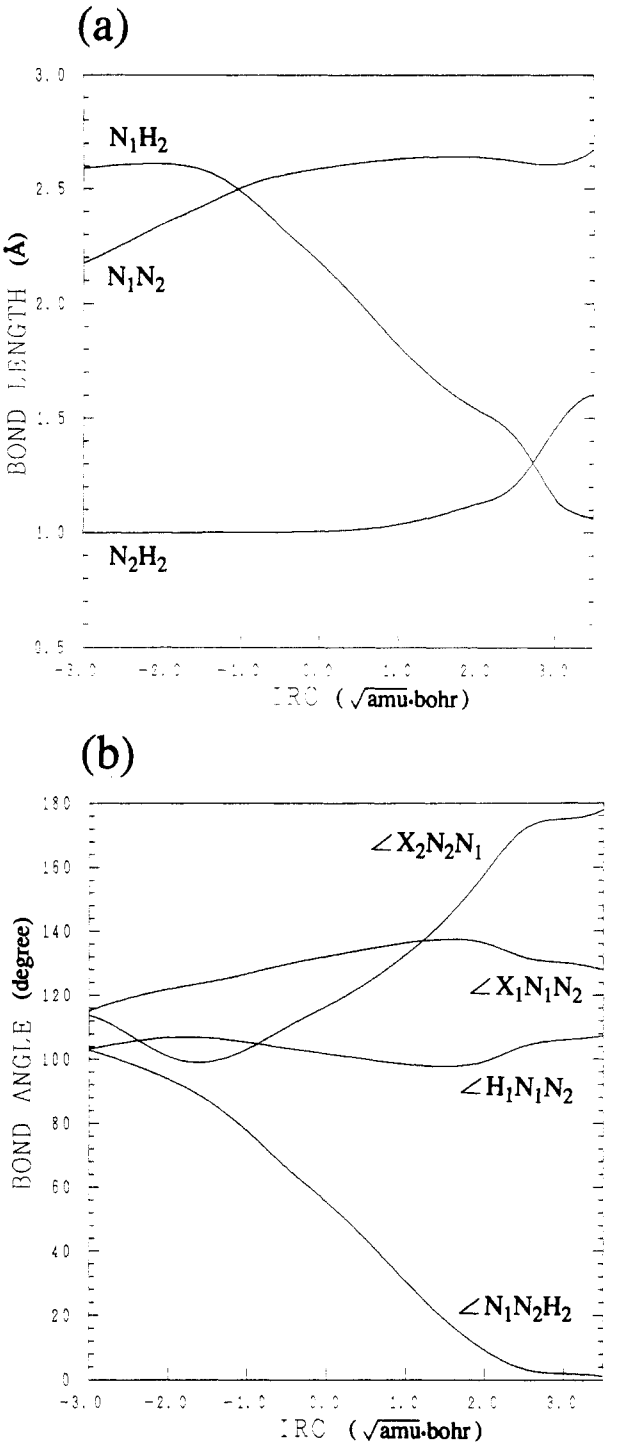

Figure 12. Geometrical changes along the IRC for the HA process: (a) bond lengths and (b) bond angles.

barrier, followed by decomposition of NH_4^+ and NH_2, with an exothermicity of 15.8 kcal/mol. Therefore, the direct $(NH_4{\cdot}NH_2)^+$ complex formation path has a thermodynamic and kinetic advantage for the PT process. On the other hand, the HA process involves $(NH_3{\cdot}NH_3)^+$ CT complex formation (Figure 15b): the CT complex does not dissociate but undergoes a rearrangement to form the $(NH_4{\cdot}NH_2)^+$ complex, which dissociates to NH_4^+ and NH_2. The overall HA process has been predicted to have no energy barrier and to be exothermic by 15.8 kcal/mol at the HF/4-31G level of calculation. This path has a thermodynamic and kinetic advantage for the HA process. This channel also corresponds to the secondary PT process, because the HA and secondary PT processes have some probabilities from the $(NH_3{\cdot}NH_3)^+$ CT complex. The ET process is a narrow channel (Figure 15c): the reactants form the CT complex, $(NH_3{\cdot}NH_3)^+$ or $(NH_4{\cdot}NH_2)^+$, which then dissociates to NH_3^+ and NH_3 with

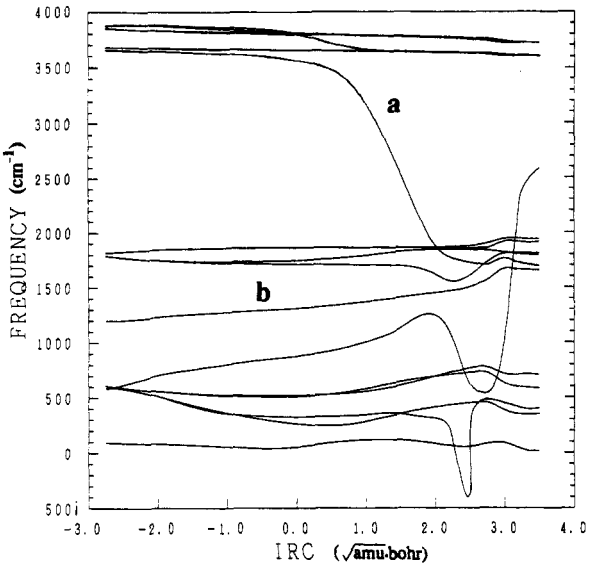

Figure 13. Frequency changes of the vibrational modes orthogonal to the IRC for the HA process.

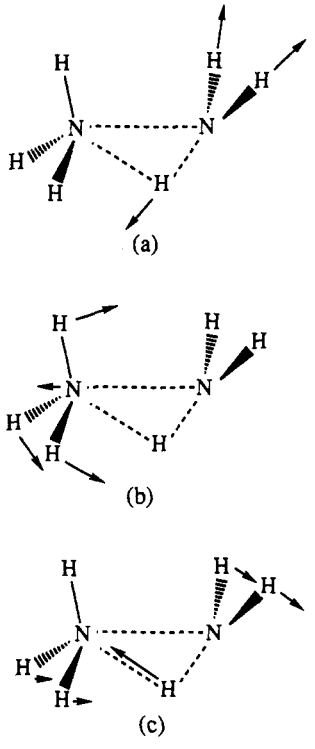

Figure 14. Displacement vectors of (a) mode a, (b) mode b, and (c) the IRC at the TS of the HA process.

an electron transferred from one to the other. If the $(NH_3 \cdot NH_3)^+$ CT complex formation and the direct $(NH_4 \cdot NH_2)^+$ complex formation have the same probabilities, PT is 75% (50% for the direct PT process and 25% for the secondary PT process), HA is 25%, and ET is 0%. These results agree well with the non-state-selected studies under thermal conditions: the reaction proceeds via PT (85%) rather than HA (15%) and ET is negligible.[3]

Conclusion

In the present work, we have proposed new reaction pathways for the vibrational-mode-specific reaction of $NH_3^+(v)$ and NH_3. We have found three TP's for the reaction: the primary TP, which is the one for CT, the geographical TP, which is the one of the potential surface, i.e., TS, and the secondary TP, which is the one for geometrical change. For the ordinary reaction coordinate, the TS merges the TP of CT and the geometrical TP, but in this case the character of the TS splits into the three TP's. The meta-IRC

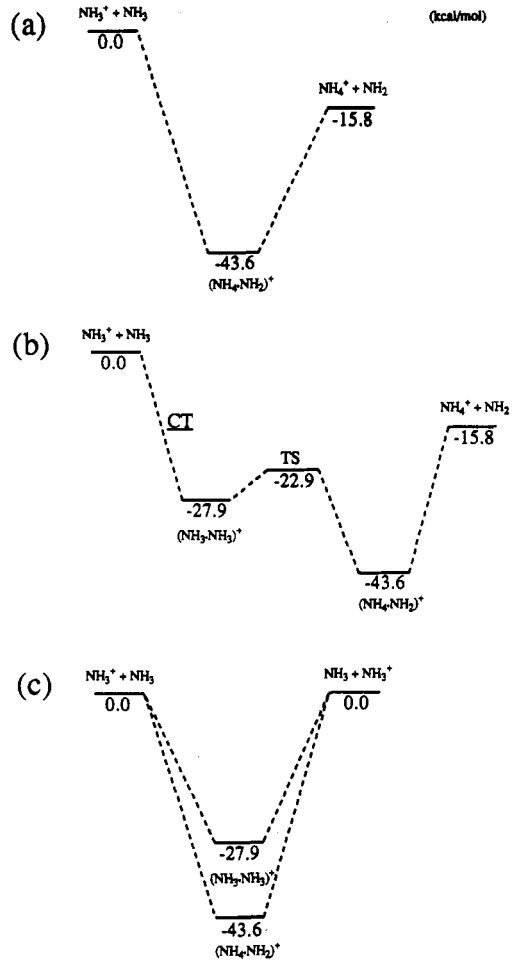

Figure 15. Energy diagram of (a) the PT process, (b) the HA process and the secondary PT process, and (c) the ET process.

for the CT complex formation reaction is characterized by the bending motions of both NH_3^+ and NN_3 in the same direction, followed by rapid CT around the primary TP, and the backward bending motion of L-NH_3 leading to the $(NH_3 \cdot NH_3)^+$ complex. The v_2 bending motion of NH_3^+ is thus parallel to the displacement vector of the meta-IRC. The v_2 bending motion can also urge the LUMO of NH_3^+ to overlap with the HOMO of NH_3, leading to significant CT from NH_3 to NH_3^+. Therefore, the excitation of the v_2 mode can promote ET and HA. On the other hand, the IRC for HA is characterized by H2 transfer toward N1 in the early stage, rotational motion of R-NH_3 around the TS, and H2 transfer from N2 to N1 on the NN axis in the last stage. It is distinctive that, instead of around the TS, the remarkable geometrical change takes place around the secondary TP. Vibrational analysis along the IRC shows that the dynamics along the IRC are not significant for vibrational-mode specificity. Therefore, we can conclude that the vibrational-mode specificity observed in ET and HA is attributable to the CT process promoted by the excitation of the v_2 vibrational mode of NH_3^+ along the meta-IRC. Moreover, our mechanism illustrates the non-state-selected experimental results: the reaction proceeds via PT (85%) rather than HA (15%) and ET is negligible.

Acknowledgment. This work was supported by a Grant-in-Aid for Scientific Research from the Ministry of Education, Science and Culture of Japan, for which we express our gratitude. The molecular orbital calculations were carried out at the Data Processing Center of Kyoto University and the Computer Center of the Institute for Molecular Science (IMS) and we thank them for their generous permission to use the FACOM M-780 and VP-400 and HITAC M-680H and S-820 computer systems, respectively. The efforts of both referees are gratefully acknowledged. Their careful reading of the original manuscript lead to many critical comments which were indeed valuable.